Theoretical analysis of fatigue failure in mechanically fastened Fibre Metal Laminate joints containing multiple cracks

Wang, Wandong; Rans, Calvin; Benedictus, Rinze

DOI
10.1016/j.engfailanal.2018.03.012

Publication date
2018

Document Version
Accepted author manuscript

Published in
Engineering Failure Analysis

Theoretical analysis of fatigue failure in mechanically fastened Fibre Metal Laminate joints containing multiple cracks

Wandong Wang[a,*], Calvin Rans[a], Rinze Benedictus[a]

[a]*Structural Integrity & Composites Group, Faculty of Aerospace Engineering, Delft University of Technology, P.O. Box 5058, 2600 GB Delft, The Netherlands*

Abstract

Mechanically fastened joints are susceptible to the presence of multiple-site damage (MSD) cracks in the critical fastener row. Different from the MSD growth in joints consisting of metallic substrates, the two coupled metal crack growth and interfacial delamination propagation failure mechanisms in Fibre Metal Laminates (FMLs) make the prediction of fatigue behaviour in FML joints with MSD scenario burdensome and impractical when considering all factors influencing the fatigue performance. This paper presents a theoretical study on the MSD crack growth behaviour in mechanically fastened FML joints with a focus of modelling the effects of bearing and bypass loads. The proposed model in this paper is built upon analytical models dealing with MSD growth in flat FML panels and single crack growth in FML panels subjected to a combined tension-pin loading case. This model would be particularly useful for symmetric FML joints where no secondary bending effects present. A deliberately designed symmetric FML joint was tested to validate the proposed model. The model captures the rapid crack growth in the vicinity of fastener holes due to bearing stresses and crack acceleration due to the interaction of cracks. It is identified that the load redistribution between intact fastener rows and the cracked fastener row accelerates crack growth with crack length. The effects of secondary bending stresses in FML joints on the crack growth behaviour is extensively discussed. The performance of the proposed model for single lap FML joints is also examined using test data from open literature. It is found that the proposed model provides a conservative prediction for the tested single shear lap FML joint from open literature.

Keywords: MSD, fibre metal laminates, mechanically fastened joints, load redistribution mechanism, crack growth acceleration

1. Introduction

Fibre Metal Laminate (FML) is a material concept comprising alternate metal sheets and composite layers. This material concept is evolved out of bonding thin metal sheets together to enhance the damage tolerance properties. The deliberately interleaved fatigue resistant fibre layers between the metal sheets in FMLs act as a second load path when fatigue cracks propagate in the metal layers, reducing the effective crack-driving force at the crack tip and prolonging fatigue life. The resultant slower and stabler crack growth behaviour in FML, in comparison with that in metals, is very desirable in the context of damage tolerance philosophy used in aerospace sector.

This fibre bridging mechanism is easy to understand but difficult to capture effectively in analysing the fatigue crack growth behaviour in FMLs. Great success of adequately capturing the bridging mechanism was only achieved until the composite nature of FML was embraced and the interplay between the fibre and metal layers was analytically described, resulting in an accurate fatigue crack growth prediction model

*Corresponding author. *Tel.:* +31 (0)15 278 9748;
E-mail address: w.wang-3@tudelft.nl, wwandong@gmail.com

for FMLs by Alderliesten [1, 2]. The crack growth in the metal layers and delamination propagation at the metal/composite interface can be simultaneously predicted. Continued effort in extending the capabilities of predicting crack growth behaviour has also been achieved by building upon Alderliesten's analytical approach. These extensions have been made to account for residual strength [3], variable amplitude loading [4–6], generalized FML configurations [7], more recently MSD scenario [8–11] and pin loading [12, 13].

It is well understood that the mechanically fastened joints are potentially vulnerable structures as a result of secondary bending, stress concentration and pin bearing effects at fastener holes. The structural behaviour of mechanically fastened FML joints therefore has been the subject of extensive research, including the static behaviour and fatigue behaviour. J.J.M. de Rijk [14] has extended the neutral line model developed by Schijve [15] to calculate the load transfer and secondary bending stresses in FML joints. The bearing strength of FMLs [16–18] and the progressive damage behaviour of pin loaded FMLs [19, 20] have been studied. The present authors have also studied the fatigue crack growth behaviour in FMLs subjected to a more representative case of a combined tension-pin loading for mechanically fastened joints [12, 13].

In particular, mechanically fastened joints are susceptible to the simultaneous presence of multiple cracks at several fastener holes in the critical row of fasteners [21–24]. In light of the introduction of Limit of Validity (LOV) concept to the airworthiness regulations that puts limitations on damage tolerance philosophy [8, 25, 26], it is crucial to examine the crack growth behaviour in mechanically fastened FML joints with MSD scenario. In this context, the present authors have developed and validated analytical models for predicting the MSD crack growth in FML plates under far-field tension [8–11] and single crack growth in FMLs subjected to a combined tension-pin loading [12, 13], with the intension of incorporating them into an analysis frame that can evaluate the MSD crack growth behaviour in FML joints. It has been identified from the previous research that both pin bearing loading and MSD crack scenario significantly accelerate the fatigue crack growth in FMLs, stimulating the motivation to investigate into the MSD crack growth behaviour in FML joints.

The crack in a mechanically fastened joint is subjected to a complex stress field. This stress field comprises stress components such as bearing, frictional forces, bypass, secondary bending stresses and residual stresses at fastener holes. Among them, pin bearing, bypass and secondary bending stresses dominate the MSD crack growth behaviour in FML joints. The aim of this paper is to propose an computationally efficient analysis frame for predicting MSD growth behaviour in mechanically fastened FML joints by systematically integrating the well established analytical models with a focus of analysing crack interaction under tensile bypass loading and pin bearing effects. This model is particularly suitable for analysing MSD growth behaviour in symmetric FML joints without secondary bending stresses. Experimental test has been carried out to validate the performance of the proposed model using the test data.

Secondary bending stresses present in most commonly used single lap joints; however, incorporating them into modelling crack growth in FMLs is highly complicated and significantly sacrifices computational efficiency. It was decided not to model secondary bending effects for the purpose of this paper. Nevertheless, the effects of secondary bending on crack growth in FML will be extensively discussed and the performance of the proposed model for a single lap FML joint will be examined using test data from open literature.

2. Background: Stresses in a mechanically fastened FML joint and their influences on crack growth behaviour

The fatigue performance of FML joints is affected by many stress components that are present due to the complexity of load transfer from one jointed FML panel to another via fastened joints. It is therefore desirable to start with an introduction of the stress components in mechanically fastened joints and their complications in developing an analytical model for predicting the MSD crack growth behaviour in such joints.

As illustrated in Fig. 1, the stresses in a joint can be broken down into stress components related to bearing, friction and bypass loading components resulting from load transfer. In addition, the stresses can comprise secondary bending stresses in mechanically fastened joints where eccentricities in load path exist, and local compressive residual stresses around the periphery of each fastener hole to which interference fit fastener or cold expansion processes are applied [27].

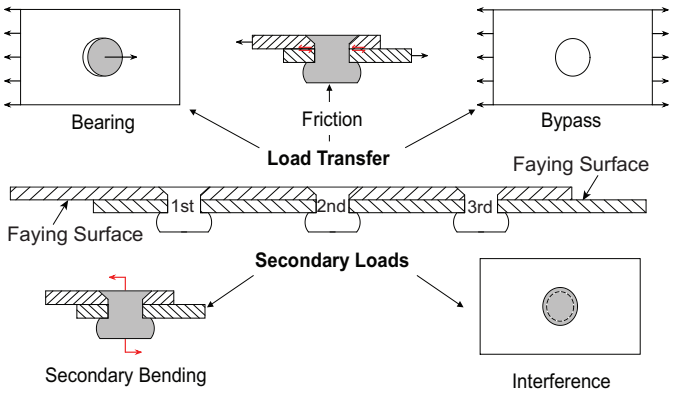

Figure 1: Loading components in a mechanically fastened joint [27]

Friction at the faying joint surfaces induces fretting damage that contributes to the fatigue crack nucleation . On the contrary, the compressive residual stresses at the fastener hole are beneficial and retard the crack nucleation. Both of them mainly affect the fatigue initiation phase [28]. It is the bearing stress and bypass loading resulting from load transfer and secondary bending that dominate the MSD crack growth behaviour in mechanically fastened FML joints. Their effects will be discussed in detail in proceeding subsections.

2.1. Load transfer

Load is transferred in a mechanically fastened joint by means of bearing between fasteners and jointed plates and friction. A significant portion of overall load is transferred by bearing while friction only accounts for a small portion. For a multiple-row joint, each row of fasteners transfers a portion of the applied load while the remainder, known as bypass load, remains in the loaded plate.

Based on the displacement compatibility between jointed plates and fasteners, closed form solutions have been derived to calculate the load transferred by each fastener row for the typical joint configuration containing three rows of fasteners [29, 30]. To aid in explanation, T_1, T_2 and T_3 are designated to loads transferred by the first, second and third fastener row respectively. In open literature, it has been shown that the outer rows transfer the same amount of load, $T_1 = T_3$, that is always more than that transferred by the middle row [14, 30].

It is obvious that the first fastener row in the upper sheet and the third fastener row in the lower sheet (Fig. 1) are the critical rows where the fastener holes subject to the highest bypass load and the highest bearing load among all fastener holes. In consequence, cracks tend to initiate at fastener hole edges in the critical fastener rows. Another significant contributor to the crack initiation in the critical fastener rows is the secondary bending stresses, which will be explained in the next subsection.

For the critical fastener row without any cracks, the total bearing load is equal to T_3, and the bypass load equals the total load transferred by other fastener rows, i.e., $T_1 + T_2$. It is important to understand that crack growth in the joint can change the bypass load and bearing load for the critical fastener row. The cracks initiating from fastener holes permit fasteners to have more freedom of rotation, indicating a higher fastener flexibility at the cracked fastener hole. Moreover, the crack growth in the critical row results in the jointed plate becoming less stiff, indicating a higher plate flexibility. Both of them lead to the cracked fastener row transferring less load and the rest fastener rows transfer more load.

Analytically estimating the sophisticated changes in the fastener flexibility and plate flexibility as a result of the crack growth in the critical row is extremely challenging and can be an extensive research topic on it own. Finite element modelling or experimental measuring techniques have to be implemented to evaluate the load transfer in a mechanically fastened joint containing MSD cracks in the critical row of fasteners.

2.2. Secondary bending

Eccentricities in the load path of a mechanically fastened joint can lead to out-of-plane displacements and bending stresses known as secondary bending. The bending stresses caused by load path eccentricities inherent to mechanically fastened joints can be estimated using the neutral line model [14, 15, 28]. For the typical three-row joint configuration illustrated in Fig. 1, the outer fastener rows encounter the highest secondary bending stresses.

The secondary bending stresses vary through the thickness of the jointed plate. Superposed upon the tensile stress resulting from the load transfer in the critical row, the bending stress leads to the faying surface experiencing the highest tensile stress. As a consequence the faying surface in the critical row is susceptible to fatigue crack nucleation and crack growth. For FMLs, the stiffness variation trough the laminate thickness has to be considered when calculating the bending stresses in FML joints [30]. An example of stress distribution through the laminate thickness in the critical row of a three-row riveted Glare3-3/2-0.3 lap joint is given in Fig. 2.

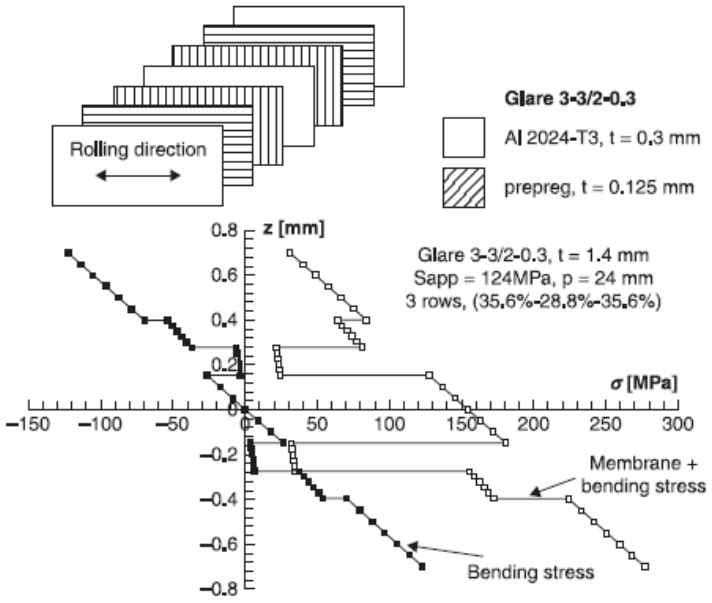

Figure 2: Illustration of the stress distribution through thickness predicted by the neutral line model for a critical rivet row of a three-row riveted Glare joint [30]

Secondary bending stresses could induce complex crack configuration in FML joints. The cracks in the metal layers originating from the same fastener hole could possess different crack lengths through the laminate thickness and different delamination shapes at the metal/composite interfaces as a consequence of the stress variation through the laminate thickness resulting from the secondary bending stresses [7], as illustrated in Fig. 2.

This effect of bending stresses poses two complications in calculating the crack growth behaviour of multiple cracks in the same fastener row. The first one is that the variation in crack lengths through the laminate thickness requires local discretization of the crack configurations in the metal sheets originating from the same fastener hole. The uncracked metal sheets in the wake of cracks in other metal sheets act as bridging materials and the local load path eccentricity leads to local bending stresses in the uncracked metal layers [7]. Special care needs to be taken to account for these effects [7]. Another complication is in the calculation of crack interaction in terms of the load redistribution mechanism detailed in [8, 10]. The presence of other cracks reduces the local geometric stiffness, resulting in load redistribution from the

cracks to a single crack for a given loading case when analysing the state of the single crack. The strain distribution derived from the Westergaard stress distribution is assumed the same through the laminate thickness in front of the crack tip of the single crack in order to evaluate the load redistribution [8]. At the location of a crack of the same length in the metal layers, the isostrain condition is applied to calculate the stress reduction, thus the load reduction, caused by the cracked metal layers. However, the complex crack configuration induced by the secondary bending stresses requires great modification of the method to evaluate the load redistribution and the effects on a single crack with different crack lengths in the metal layers.

It is important to make a distinction between the load redistribution among multiple cracks and the load redistribution over multiple fastener rows. The later is due to the changes in the plate flexibility and fastener flexibility caused by the multiple cracks. For a given load transfer over multiple fastener rows, the load redistribution from other cracks to a single crack needs to be evaluated in order to calculate the state of the single crack.

3. Model implementation

From the previous section, it can be concluded that developing an analytical model to consider the influences of load transfer over multiple rows and secondary bending on MSD crack growth in an FML joint is burdensome and impractical. A simplified prediction model based on the prediction models developed by the present authors in [8, 10] and [13] is therefore proposed with some assumptions and simplifications that will be described in the following subsection.

For the clarity and completeness of this paper, the calculation method for a single symmetric crack in an FML subjected to a combined tension-pin loading is briefly summarized, then the method is extended for a non-symmetric crack, and for MSD cracks in a mechanically fastened FML joints.

3.1. Assumptions and simplifications

Calculating the load transfer over multiple rows in a mechanically fastened joint containing MSD cracks in the critical row is an extensive research topic on it own. The load redistribution over multiple fastener rows will not be simultaneously considered when calculating the crack states in the critical fastener row in this proposed model. The initial load transfer over multiple rows can be calculated using the closed form analytical equations [29, 30]. The calculated load transfer in each row can then be used to obtain the bypass load and bearing load for the critical fastener row, which are the input parameters for calculating the crack growth behaviour in the proposed model.

The secondary bending effects can result in a complex fatigue crack configuration through the laminate thickness. Calculating the state of a complex fatigue crack configuration in an FML requires the implementation of the Wilson's model [7] at the cost of great computational efficiency. In order to derive a computationally efficient model to evaluate the MSD crack growth behaviour in FML joints, the secondary bending effects are neglected in the model, but will be qualitatively analysed in Section 5.

In consequence of the assumptions and simplification, cracks in the critical fastener row are subjected to the calculated pin bearing loading and bypass loading. The methodology adopted in [8, 10, 13] will be followed here: LEFM and the principle of superposition are applied to calculate the crack growth in the metal layers and the delamination growth at the metal/composite interfaces.

3.2. Single symmetric crack

An analytical model has been developed for calculating the crack state of a single symmetric crack in an FML subjected to pin loading and far-field tension (see Fig. 3). One is referred to the papers [12, 13] by the present authors for detailed description of the model.

The overall stress intensity factor, K_{joint}, at the crack tip in the metal layers is expressed as the following equation:

$$K_{joint} = K_{bypass} + 0.5K_{pin,ff} + 0.5K_{pin,bearing} \tag{1}$$

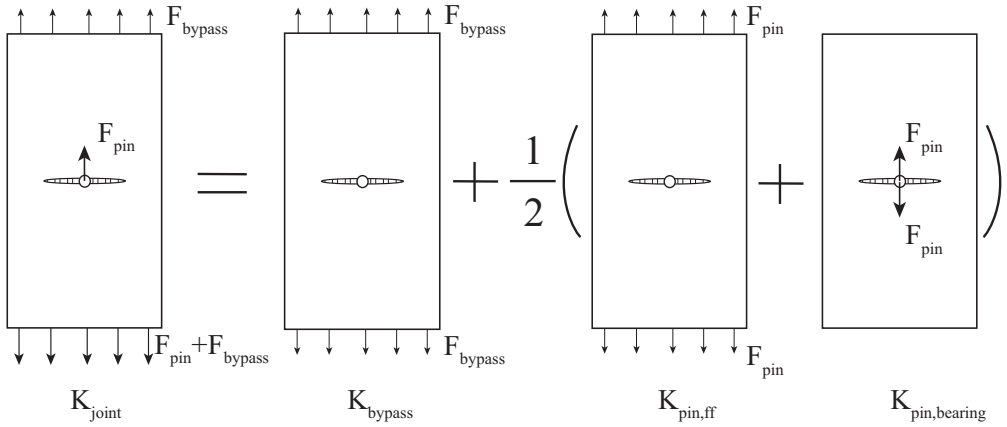

Figure 3: Superposition scheme of the overall stress intensity factor for a single symmetric crack in an FML

The superposition of the stress intensity factors is illustrated in Fig. 3. It is important to understand that each of the stress intensity factors on the right side of Eq. 1 can be decomposed into two items. The first item is the stress intensity factor due to the stress in the metal layers resulting from one corresponding loading case, while the second item is the stress intensity factor due to the fibre bridging mechanism. In order to avoid repetitively calculating the bridging mechanism and thus the stress intensity factors due to the bridging mechanism for each loading case, an alternative method has been proposed in paper [13]: K_{joint} can be alternatively expressed as:

$$K_{joint} = K_{app} + K_{br} \tag{2}$$

where K_{app} denotes the sum of stress intensity factors due to the loading cases acting on the single crack, which is given by Eq. 3. K_{br} is the stress intensity factor due to the fibre bridging mechanism.

Each of the stress intensity factors on the right side of Eq. 3 is a function of the stress in the metal layers resulting from the corresponding loading component illustrated in Fig. 3 [31]. The superscript * is added to make a distinction between these stress intensity factors and the total stress intensity factors in Eq. 1.

$$K_{app} = K^*_{bypass} + 0.5K^*_{pin,ff} + 0.5K^*_{pin,bearing} \tag{3}$$

The calculation of K_{br} is achieved by solving for the bridging stress distribution, $S_{br}(x)$, and integrating the stress intensity factor due to the bridging stress over the whole delamination [31]. The calculation of $S_{br}(x)$ is implemented by applying the principle of displacement compatibility [2, 31]. The total crack opening in the metal layers including the opening component $v_{app}(x)$ due to applied load and closing component $v_{br}(x)$ due to the bridging stresses should be compatible with the total deformation of the delaminated fibre layer due to elongation $\delta_f(x)$ and shear deformation $\delta_{pp}(x)$. This displacement compatibility is expressed as Eq. 4.

$$v_{app}(x) - v_{br}(x) = \delta_f(x) + \delta_{pp}(x) \tag{4}$$

Analogous to the decomposition of K_{app}, the total crack opening displacement, v_{app}, is also broken down into contributing factors related to the corresponding loading cases illustrated in Fig. 3.

$$v_{app}(x) = v^*_{bypass}(x) + 0.5v^*_{pin,ff}(x) + 0.5v^*_{pin,bearing}(x) \tag{5}$$

Not only is the prediction of the crack propagation in the metal layers indispensable but also the prediction of the interfacial delamination for fatigue failure analysis of FMLs. Strain energy release rate, $G(x)$, is applied to characterize the state of the delamination. Once the bridging stress distribution, $S_{br}(x)$, is determined, the strain energy release rate, $G(x)$, can be calculated using Eq. 6.

$$G(x) = \frac{n_f t_f}{2jE_f}\left(\frac{n_m t_m E_m}{n_m t_m E_m + n_f t_f E_f}\right)(S_f(x) + S_{br}(x))^2 \tag{6}$$

The detailed solutions of Eqs. 2-6 can be found in the work [13, 31] by the present authors.

3.3. Single non-symmetric crack

As illustrated in Fig. 4, the non-symmetric crack configuration is a more generic configuration in comparison with the symmetric crack configuration in the previous subsection. For a non-symmetric crack in an FML subjected to pin loading and far-field tension, the same approach in the previous subsection can be followed to calculate K_{joint} and G_x. Nevertheless, it is noted that the states of the two tips of the non-symmetric crack are not identical as a result of the crack tip non-symmetry, the delamination non-symmetry and the non-symmetric pin loading effects for the two crack tips (see Fig. 4) [31].

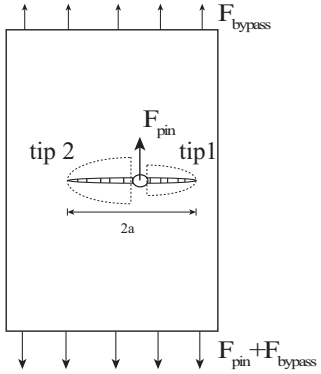

Figure 4: A non-symmetric crack in an FML subjected to pin loading and far-field tension

Consequently, two overall stress intensity factors have to be used to characterize the states of the two crack tips. In the same manner as described in the previous subsection, the overall stress intensity factor for crack tip 1, $(K_{joint})_1$, can be expressed as:

$$(K_{joint})_1 = (K_{app})_1 + (K_{br})_1 = (K^*_{bypass} + 0.5K^*_{pin,ff})_1 + 0.5(K^*_{pin,bearing})_1 + (K_{br})_1 \tag{7}$$

and the overall stress intensity factor, $(K_{joint})_2$, for crack tip 2 can be expressed as:

$$(K_{joint})_2 = (K_{app})_2 + (K_{br})_2 = (K^*_{bypass} + 0.5K^*_{pin,ff})_2 + 0.5(K^*_{pin,bearing})_2 + (K_{br})_2 \tag{8}$$

where the subscripts $_1$ and $_2$ are employed to indicate that the variables are related to crack tip 1 and crack tip 2 respectively. It is crucial to highlight that the corresponding stress intensity factors of the two crack tips in Eq. 7 and Eq. 8 are not identical. The calculation approach for $(K^*_{bypass} + 0.5K^*_{pin,ff})_1$ and $(K^*_{bypass} + 0.5K^*_{pin,ff})_2$ due to far-field tension has been dedicatedly described in [31] by the present authors.

Eq. 4 and Eq. 5 can be used to calculate the asymmetric bridging stress distribution, $S_{br}(x)$, and the resultant $(K_{br})_1$ and $(K_{br})_2$ [31]. The asymmetric crack opening, $v^*_{bypass}(x) + 0.5v^*_{pin,ff}(x)$, due to far-field loading can be derived using the same approach detailed in [31].

The stress intensity factors $(K_{pin,bearing})_1$ and $(K_{pin,bearing})_2$ resulting from the pin bearing are different and the opening $v^*_{pin,bearing}$ is not symmetric since the crack tips are not symmetric with respect to the pin hole (see Fig. 4). Based on the work pertaining to the analysis of the pin loading effects on the crack state of a symmetric crack in an FML in [12, 13], a pair of pin bearing loads acting on the crack flanks of a through thickness crack in an FML can be modelled as a pair of point loads and are assumed to be borne by the metal layers only. A generic illustration of a pair of point loads acting on the crack flanks of a crack is depicted in Fig. 5.

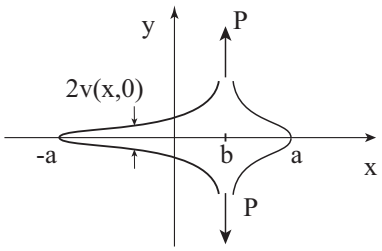

Figure 5: Illustration of a pair of point loads acting on crack flanks [32]

The stress intensity factors, $(K^*_{pin,bearing})_1$ and $(K^*_{pin,bearing})_2$, for the two crack tips illustrated in Fig. 4 can be expressed with the following equations:

$$(K^*_{pin,bearing})_1 = \frac{P}{\sqrt{\pi a}} \frac{\sqrt{a^2 - b^2}}{a - b} \tag{9}$$

$$(K^*_{pin,bearing})_2 = \frac{P}{\sqrt{\pi a}} \frac{\sqrt{a^2 - b^2}}{a + b} \tag{10}$$

and the crack opening displacement of the crack, $v^*_{pin,bearing}$, can be written as:

$$v^*_{pin,bearing} = \frac{2P}{\pi E_m} cosh^{-1} \frac{a^2 - bx}{a|x - b|} \tag{11}$$

with E_m being the Young's modulus of the metallic panel. The crack length a, the location, b, and load, P, are illustrated in Fig. 5.

For the non-symmetric crack illustrated in Fig. 4, the location of the pair of point loads, b, can be determined according to the geometric relation between the pin hole and the two crack tips. The point load, P, for each metal layer can be given by:

$$P = \frac{F_{pin}}{n_m t_m} \tag{12}$$

where n_m denotes the number of the metal layers and t_m denotes the thickness of each metal layer.

3.4. MSD cracks

Fig. 6 illustrates the decomposition of the pin loading and far-field tension acting on MSD cracks in an FML into simpler symmetric loading cases. For each crack tip, a set of stress intensity factors can be derived for the corresponding loading cases and superposed, following the same basic approach as described in subsection 3.2. The derivation of the stress intensity factors for the tip on the right side of crack i, denoted with the subscript $_{i1}$, is described in this subsection as an example.

The decomposition of the stress intensity factor, $(K_{joint})_{i1}$, for crack tip $i1$, as illustrated in Fig. 6, can be written as:

$$(K_{joint})_{i1} = (K_{bypass} + 0.5K_{pin,ff})_{i1} + 0.5(K_{pin,bearing})_{i1} \tag{13}$$

In order to avoid repetitively calculating the bridging stress distribution for the same crack configuration for different loading cases, the above equation is alternatively given as:

$$(K_{joint})_{i1} = (K_{app})_{i1} + (K_{br})_{i1} \tag{14}$$

with

$$(K_{app})_{i1} = (K^*_{bypass} + 0.5K^*_{pin,ff})_{i1} + 0.5(K^*_{pin,bearing})_{i1} \tag{15}$$

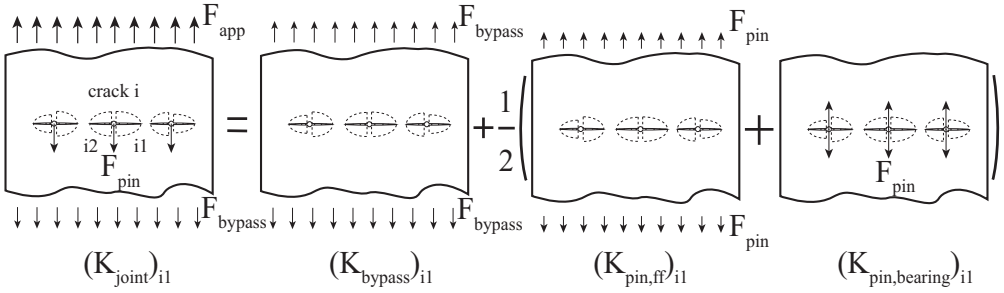

Figure 6: Superposition scheme of loading cases for MSD cracks in an FML

The corresponding crack opening displacement of the single crack i, $(v^*_{app}(x))_i$, is expressed as:

$$(v_{app}(x))_i = (v^*_{bypass}(x) + 0.5v^*_{pin,ff}(x))_i + 0.5(v^*_{pin,bearing}(x))_i \tag{16}$$

When analysing the crack state of the single crack i, the adjacent cracks are treated as local stiffness reductions in this research [8, 10, 11]. The reductions in local stiffness lead to load redistribution from the adjacent cracks to the single crack, enlarging the stress intensity factor and the corresponding crack opening of the single crack in comparison with the isolated crack scenario.

$(K^*_{bypass} + 0.5K^*_{pin,ff})_{i1}$ results from the far-field loading cases illustrated in Fig. 6. The calculation of it involves considering the load redistribution mechanism, which is described in detail in [10]. Two different Westergaard stress distributions in front of the single crack can be applied to evaluate the load redistribution as a result of the reductions in local stiffness induced by the presence of the adjacent cracks. Following the methodology in [10], $(K^*_{bypass} + 0.5K^*_{pin,ff})_{i1}$ and $(v^*_{bypass}(x) + 0.5v^*_{pin,ff}(x))_i$ can be calculated.

The significance of modelling the load redistribution mechanism under far-field tension has been demonstrated in [10]. The significance of modelling it in calculating $K^*_{pin,bearing}$ for the case of MSD cracks subjected to pairs of point loads has not been fully evaluated.

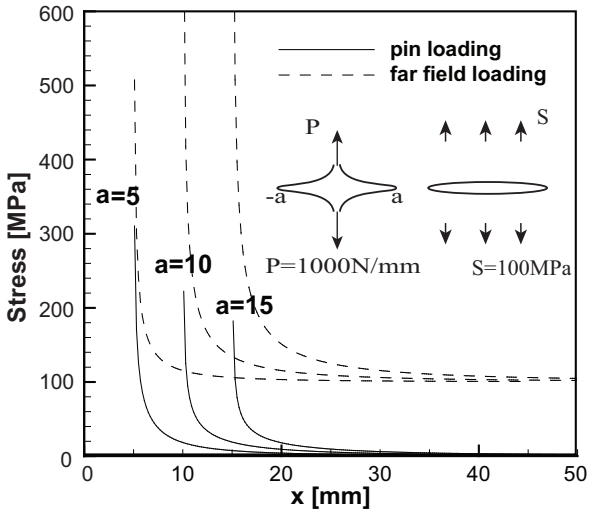

Figure 7: Comparison of stress distributions ahead of a crack tip for a far-field tension of $S = 100\ MPa$ and for a pair of point loads with $P = 1000\ N/mm$ for different crack lengths

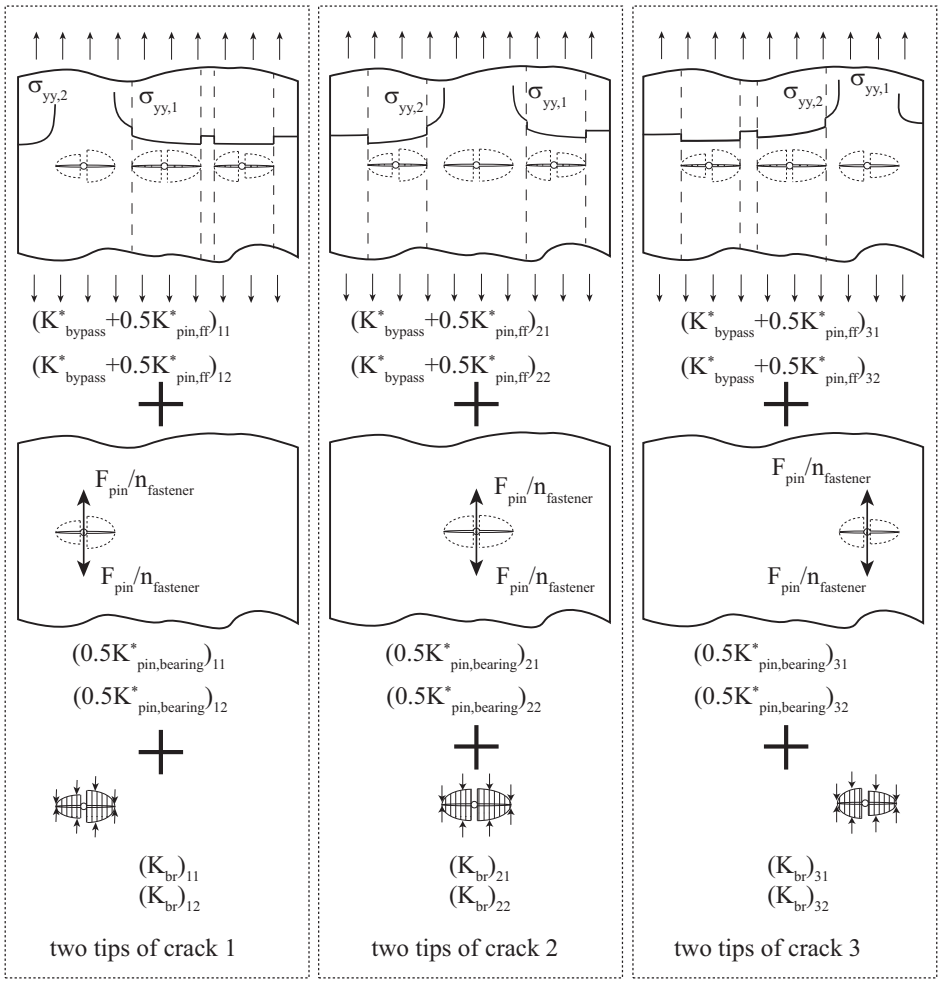

Figure 8: Illustration of sequential analysis of each crack state

The stress distribution in front of the tip of a crack loaded by a pair of point loads, illustrated in Fig. 5, can be given as:

$$\sigma_{yy} = \frac{P}{\pi} \frac{\sqrt{a^2 - b^2}}{(x-b)\sqrt{x^2 - a^2}} \tag{17}$$

In Fig. 7, the stress distributions in front of a crack in an infinite panel subjected to a pair of point loads acting at the center of the crack ($b = 0$) are compared to the stress distributions of the crack subjected to far-field tensile stress for different crack lengths. Typical quantities for the pin load and far-field stress are chosen respectively. As can be seen, the magnitude of the stress distribution in front of the crack subjected to a pair of point loads is much lower than that of the same crack subjected to far-field loading, the stress roughly 15 mm away from the crack tip gets close to 0 MPa. The scale of the stress distribution for the case of far-field loading escalates with increasing crack length. On the contrary, in case of a pair of point loads, the stress distribution magnitude decreases with crack length, as shown in Fig. 7.

Based on the comparison and analysis, it is concluded that the load redistribution caused by the presence of other cracks millimeters away in front of a crack loaded by a pair of point loads is negligible for FMLs. Modelling this load redistribution is feasible, but doubles the computation without improving the precision of the model. Consequently, the calculation of $K^*_{pin,bearing}$ and $v_{pin,bearing}(x)$ for each of the multiple cracks

therefore can be derived by considering each crack as an isolated crack under a pair of point loads.

It is noteworthy that the point load, P, for the MSD scenario should be calculated with the following equation:

$$P = \frac{F_{pin}}{n_{fastener} n_m t_m} \tag{18}$$

with $n_{fastener}$ denoting the number of fastener holes.

The overall approach for calculating the crack states of MSD cracks in an FML joint is summarized in Fig. 8. Fatigue crack growth prediction is an iterative process for FMLs, the crack state and corresponding delamination state of each crack in the FML joint with MSD cracks can be used to predict the propagation rates of the two failure mechanisms using the empirical Paris equations [10, 11]. A new crack state would be obtained. The above mentioned procedure is applied to calculate the new crack state. The calculation will stop until two crack tips coalesce.

4. Model validation for a joint without secondary bending

A mechanically fastened FML joint was designed and tested to verify the performance of the proposed methodology. The configuration of the FML joint is illustrated in Fig. 9. The joint was designed with the intention to exclusively present the stress components that are accounted for by the proposed methodology. Secondary bending which is not taken into account is avoided in the joint. The test data acquired with this FML joint would provide a more accurate validation of the present model.

4.1. Test procedure

Standard Glare [33], one variant of FML, was used to manufacture the joint. The layup of the used Glare3 3/2-0.4 panel is [Al/0/90/Al/90/0/Al] with 90 and 0 indicating the orientation of S2-glass fibres embedded in FM94 epoxy resin system. The thickness of the aluminium sheet is 0.4 mm. The material properties of the prepreg and aluminium are summarized in Table 1.

Two Glare3 3/2-0.4 specimens were symmetrically jointed to the middle plate which was manufactured by bonding two Glare3 3/2-0.4 panels together. As a consequence the stiffness of the middle plate is equivalent to the total stiffness of the two specimens. Two fastener rows were applied such that each row transfers 50 percent of the applied load from the middle plate to the two specimens when there are no cracks in the joint.

Each fastener row had three evenly spaced fastener holes with the middle hole at the middle of each specimen as shown in Fig. 9(b). The fastener pitch was 30 mm. The fastener hole was firstly drilled and later reamed to the diameter of 4.8 mm that is the diameter of used fasteners. Therefore no compressive residual stresses at the fastener holes would present. As shown in Fig. 9(b), saw-cuts were applied to the fastener holes in the second fastener row in both specimens. The length of the saw-cut was 2.1 mm. Hi-lok HL12V6 fasteners were used to join the specimens and the middle plate. The Hi-Lok collar was not driven to the maximum protrusion but tightened enough so that the out-of-plan displacement of the specimens

Table 1: Material properties [8]

	Al	**Prepreg**
Young's modulus $E_x[GPa]$	72.4	48.9
Young's modulus $E_y[GPa]$	72.4	5.5
Shear modulus $G_{xy}[GPa]$	27.6	5.55
Poisson's ratio v_{xy}	0.33	0.33
Poisson's ratio v_{yx}	0.33	0.0371
Thickness of single layer$[mm]$	0.4	0.133
Thermal expansion coefficient[1/℃]	$22 \cdot 10^{-6}$	$6.1 \cdot 10^{-6}(0°)$ $26.2 \cdot 10^{-6}(90°)$

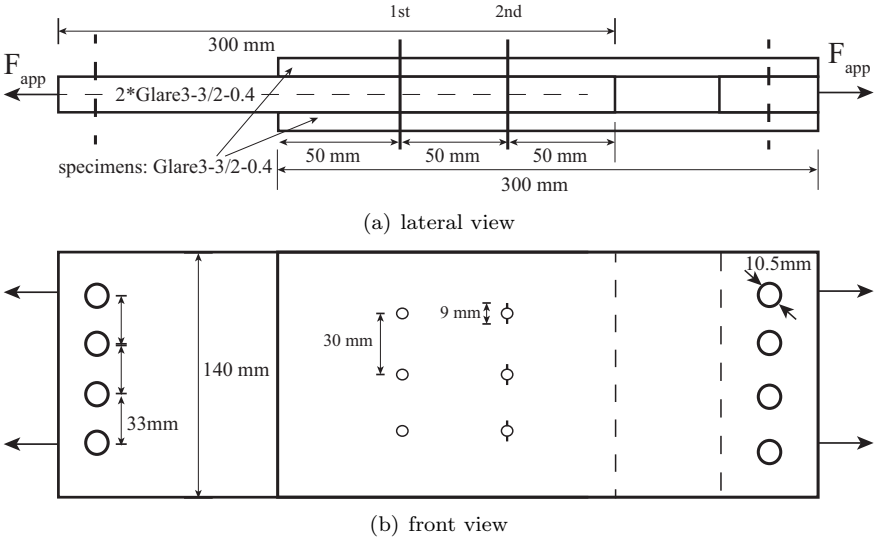

(a) lateral view

(b) front view

Figure 9: Illustration of the double shear lap FML joint

were eliminated by the collar and the head during fatigue loading. The intension was to avoid friction at the joint faying surfaces as much as possible.

The fatigue test was conducted on an MTS 810 servo-hydraulic test frame with pin hole clevis and a 250 kN load-cell (model 661. 22D-01). The maximum applied stress was $100MPa$ with a stress ratio of $R = 0.05$ and a frequency of $f = 10Hz$. The fatigue test was paused after a number of fatigue loading cycles, the maximum load was applied to make the crack fully open. Pictures of the surfaces of the specimens were taken by two high resolution cameras. The corresponding fatigue life was also recorded. The test was resumed then. The crack lengths at different fatigue life were measured from the pictures. Seven-point incremental polynomial method recommended in the ASTM E647-00 [34] was applied to reduce the scatter of the calculated crack growth rates for respective cracks.

4.2. Validation

The test data is used to validate the proposed model. In the tested joint, the bypass load and pin bearing load for the multiple cracks in the second fastener row kept changing as cracks grew. However, this changing due to the load redistribution over the two fastener rows is not simultaneously modelled when calculating the growth of multiple cracks in the proposed model.

A tension-pin loading case is required in the proposed model as input parameters in order to calculate the state of MSD cracks in an FML joint. Five tension-pin loading cases are studied for different initial crack configurations in order to directly illustrate the effects of the load redistribution among the fastener rows on the crack growth behaviour. The studied loading cases for the 2nd fastener row in the tested joint configuration are summarized in Table 2. Loading case 1 is based on the fact that the symmetry of the joint permits each fastener row to transfer 50% of the applied load, particularly when the crack length is very small. As the lengths of the cracks in the 2nd fastener row increase, the escalation in the fastener and plate flexibility allows the first row to transfer more and more load. Consequently the bypass load for the 2nd fastener row increases while the pin load decreases. Loading cases 2-4 follows this rule of thumb. Loading case 5 is to demonstrate the impact of a significant increase in the bypass load on the crack growth behaviour with long crack lengths.

In Fig. 10, the measurements and the prediction results of the five loading cases are plotted. The locations of the fastener holes and saw-cuts are indicated in both sub-figures.

The measured and predicted crack growth rates for the symmetric crack tip pairs are compared in Fig. 10(a). The test data shows that the crack growth rates are rapid in the vicinity of the fastener hole,

Table 2: Loading cases for the 2nd fastener row

case	pin load (% of applied load)	bypass load (% of applied load)	initial average crack length (mm)
1	50	50	5.0
2	49	51	6.4
3	45	55	9.1
4	40	60	10.8
5	30	70	10.8

become stable after a certain amount of crack increment and soar up when two crack tips approach each other. For the outer crack tips, a_{12} and a_{31}, their crack growth rates increase because they approach the free edge boundaries ahead and the link-up of the inner crack tips results in the two tips being the tips of a lead crack in the laminate.

The predicted crack growth behaviour for loading case 1 in Table 2 captures the trend of the growth behaviour of the multiple cracks in the tested joint. The prediction results for the crack tips near the fastener holes correlate very well with the test results. The predicted crack growth rates are very high but decrease dramatically with increasing crack length, which is consistent with test and prediction data in [12, 13] and can be attributed to the effects of pin loading in the vicinity of a fastener hole. This accurate prediction results for the crack tips in the vicinity of fastener holes is attributed to the fact that the small cracks in the second fastener row hardly altered the portions of the load transferred by the two fastener rows. When the crack lengths are long enough, the prediction results of loading case 1 under estimates the surge in the measured crack growth rate though the predicted crack growth rates of two approaching crack tips soar up. This underestimation is contrary to the over-predicted crack growth rates for FMLs containing multiple cracks subjected to far-field tensile fatigue loading in [10].

Loading case 2 for an initial crack length of 6.4 mm takes the load redistribution over the two fastener rows into consideration, the result shows that a slight rise in the bypass load for the cracks in the 2nd row can significantly enhance the predicted crack growth rates. For even longer crack lengths, the significant rise in the bypass load, however, marginally enhances the predicted crack growth rate (see the prediction results of loading cases 3-5 in Fig. 10(a)).

The corresponding predicted a-N curves for the 5 loading cases are compared to the test data in Fig. 10(b). As can be seen, the prediction model becomes conservative if the load redistribution over the fastener rows due to the crack growth in the 2nd fastener row is taken into consideration.

5. Model validation for a joint with secondary bending

This section discusses the difference between the measured crack growth rates of cracks in a single shear lap joint where the secondary bending stresses affect the crack growth behaviour and the predicted results without considering the effects of secondary bending.

The test data is extracted from the experimental study conducted by Müller [30]. Results of test series 4 from the study of fatigue behaviour of Glare3 riveted lap joints are selected for the purpose of this section. The tested joint consisted of two Glare3 3/2-0.3 sheets jointed with three rows of rivets (see the inset in Fig. 11) while each row had three rivets. The width of the Glare3 sheet was 72 mm. The loading parameters are given in Fig. 11.

The compiled crack growth rates in the metal layers of the top sheet in the joint riveted with the squeeze force of 15.6 kN are given in Fig. 11. Crack growth were measured only for the central rivet in the critical row with eddy current non-destructive inspection technique [30]. The half crack length was measured from the rivet hole edge to the crack tip. The accuracy of the test data is limited because the inspection method for invisible cracks is poor [30] and the obtained data points are few. Layer 1 had the highest tensile stress due to the secondary bending stresses (see Fig. 2), the crack initiated in layer 1 at first. However the crack growth in this layer in the beginning was very slow as a result of compressive residual stress due to high

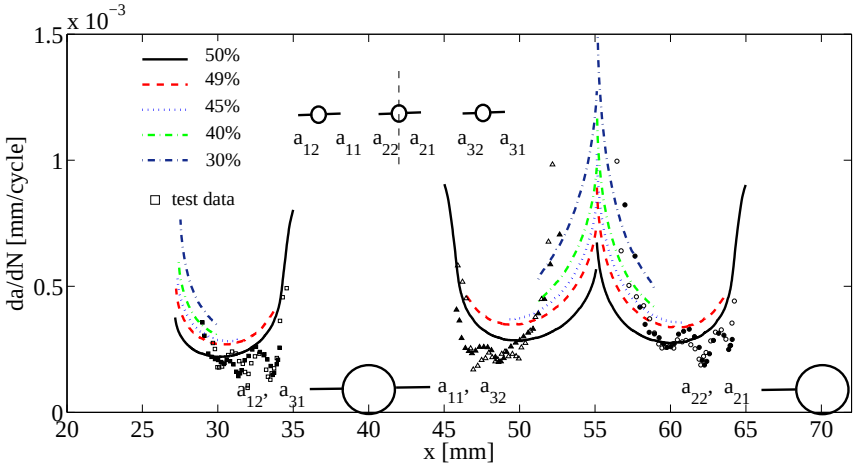

(a) Comparison of measured crack growth rates and prediction results for 5 different loading cases (% denotes the pin load for the 2nd fastener row which is a percentage of applied load)

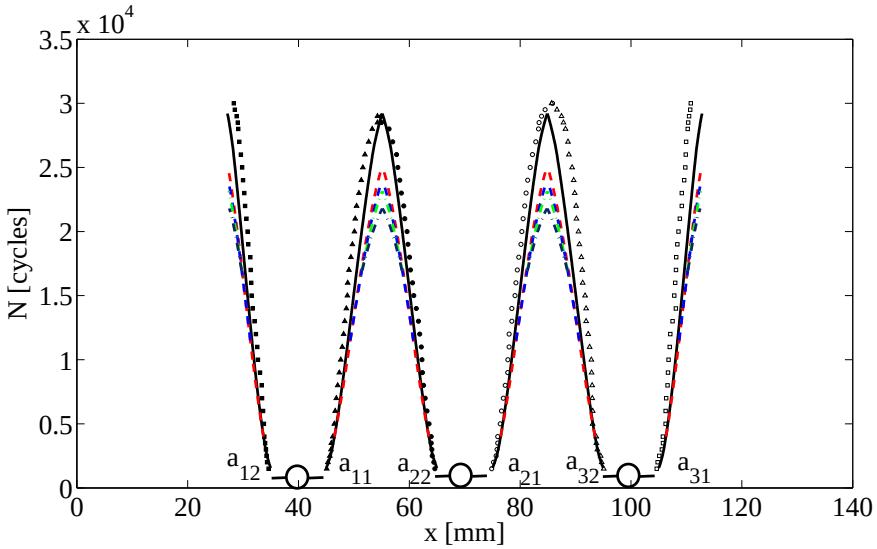

(b) Comparison of measured a-N curves and prediction results for the corresponding loading cases

Figure 10: Predictions vs test results

riveting squeeze force and the bridging mechanism provided by fibre layers and intact layer 2 and layer 3 (larger crack free life due to secondary bending in these two layers). The crack growth rate in layer 2 was higher compared to that in layer 1. Layer 3 had the highest crack growth rate due to the fact that layer 1 had been completely cracked and layer 2 was partially cracked. However, compressive bending stresses resulting both from the eccentric load paths in the joint (see the inset in Fig. 11) and the neutral line step in the partially cracked laminate (see Fig. 12) play a beneficial role in constraining the crack growth rate in layer 3.

The analysis model does not take the effects of squeeze force and the effects of secondary bending into consideration, it is assumed that cracks initiate in all metal layers simultaneously, i.e. a through thickness crack. The load distribution over the fastener rows can be calculated for the tested joint without cracks, i.e. $T_1 = 4.366kN$ and $T_2 = 4.053kN$. For this given load transfer in the joint, the bypass and pin loads

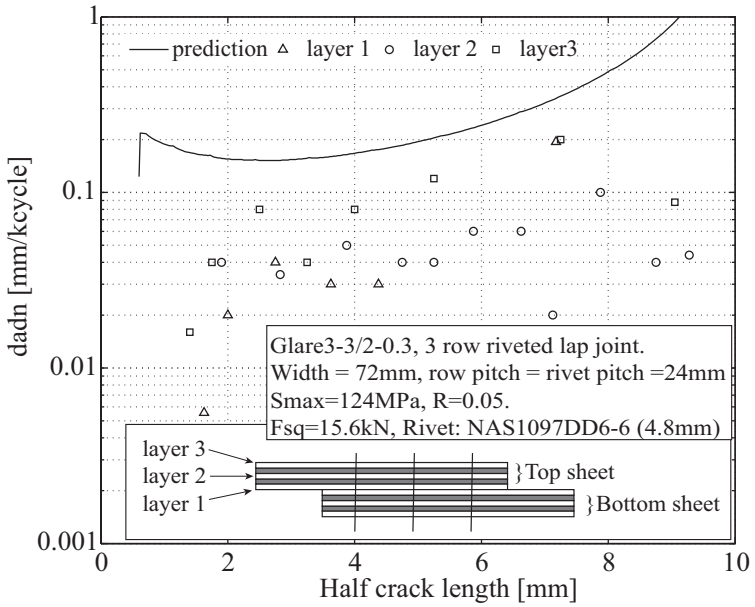

Figure 11: Comparison of crack growth rates of 3 layers in the top sheet

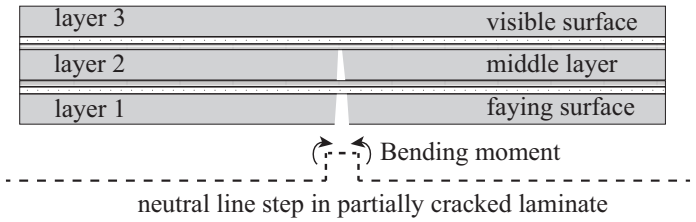

Figure 12: Local bending around crack due to neutral line step in partially cracked laminate

for the multiple cracks can be calculated. The predicted crack growth rate for the middle crack is plotted in Fig. 11. Clear difference can be observed compared to the test data since the prediction model leaves out the influence of bending stresses on the growth behaviour in different layers. It is noteworthy that the greatly simplified prediction model provides conservative prediction results.

This simplified model is very efficient to analyse the crack growth behaviour in an FML joint with MSD cracks. It avoids further discretization of the crack configuration in order to detailedly analyze the bridging mechanism offered by uncracked metal layers and the effects of local secondary bending stresses on the crack growth behaviour. It could be potentially useful for quick screening FML joint design.

6. Conclusion

The proposed methodology for analysing MSD crack growth in mechanically fastened FML joints is built upon the analytical models dedicated to individual failure mechanisms. The systematic integration of the analytical models to develop a new model is based on the principle of superposition used in linear elastic fracture mechanism. The proposed analysis methodology does not account for load redistribution over multiple fastener rows as a result of cracks evolution in one fastener row and the effects of secondary bending stresses. For a given load transfer in the joint, the overall stress intensity factor at a crack tip can be calculated by superposing the stress intensity factors resulting from different loading cases. And then the

crack growth rate can be determined. The crack state needs to be estimated one by one until all the crack states are determined for a MSD configuration.

The prediction without considering load redistribution over multiple fastener rows provide decent prediction results. It captures the feature of rapid crack growth in the vicinity of fastener holes due to pin loading, but starts to underestimate the crack growth rates after several millimeters crack growth. However, the underestimation can be alleviated by reevaluating the load transfer in the joint. Since the pin loading effects dramatically diminish with increasing crack length, the bypass load introduced by other fastener rows starts to dominate the crack growth behaviour. The increase in the bypass load therefore can improve the prediction results for MSD cracks with longer crack lengths, resulting in a more conservatively predicted fatigue growth life. In order to obtain more accurate prediction results for FML joints containing MSD cracks, the prediction methodology should simultaneously accounts for the load redistribution over multiple fastener rows when analysing the crack growth in the critical fastener row.

The secondary bending effects due to the eccentricities in the load path in single-shear lap joints induce complex crack configuration in FMLs. Even though the secondary bending effects are neglected in the proposed methodology, it provides conservative prediction results for FML single-shear lap joints based on the comparison between prediction and test data from open literature. The slow crack growth in different metal layers compared to the prediction can be attributed to several aspects. The secondary bending results in highest tensile stresses at the faying metal layer and least tensile stress in the outer metal layer (Fig. 2). This stress distribution though the laminate thickness results in the cracks in different layers having different crack lengths. The uncracked metal material in the wake of cracks in other layers could still bridge the crack, alleviating the adverse effects posed by secondary bending on the crack growth in the faying layer in an FML lap joint. For the crack growth in the outer metal layer, the secondary bending stresses resulting from the eccentricities in the load path of the joint and the neutral line step in the partially cracked laminate could play beneficial role in restricting the crack growth in this layer.

References

[1] R. C. Alderliesten. *Fatigue crack propagation and delamination growth in GLARE*. PhD thesis, Delft University of Technology, Delft, the Netherlands, 2005.

[2] R. C. Alderliesten. Analytical prediction model for fatigue crack propagation and delamination growth in glare. *International Journal of Fatigue*, 29(4):628–646, 2007.

[3] R. Rodi. *The Residual Strength Failure Sequence in Fibre Metal Laminates*. PhD thesis, Delft University of Technology, Delft, the Netherlands, 2012.

[4] S. U. Khan, R. C. Alderliesten, C. D. Rans, and R. Benedictus. Application of a modified wheeler model to predict fatigue crack growth in fibre metal laminates under variable amplitude loading. *Engineering Fracture Mechanics*, 77(9):1400–1416, 2010.

[5] S. U. Khan, R. C. Alderliesten, and R. Benedictus. Delamination in fiber metal laminates (glare) during fatigue crack growth under variable amplitude loading. *International Journal of Fatigue*, 33(9):1292–1303, 2011.

[6] S.U. Khan. *Fatigue Crack and Delamination Growth in Fibre Metal Laminates under Variable Amplitude Loading*. PhD thesis, Delft University of Technology, Delft, the Netherlands, 2013.

[7] G. Wilson. *Fatigue crack growth prediction for generalized fiber metal laminates and hybrid materials*. PhD thesis, Delft University of Technology, Delft, the Netherlands, 2013.

[8] W. Wang, C. Rans, R. C. Alderliesten, and R. Benedictus. Predicting the influence of discretely notched layers on fatigue crack growth in fibre metal laminates. *Engineering Fracture Mechanics*, 145:1–14, 2015.

[9] W. Wang, C. Rans, R.C. Alderliesten, and R. Benedictus. Philosophy of multiple-site damage analysis for fibre metal laminate structures. In *Proceedings of 28th Symposium of the International Committee on Aeronautical Fatigue ICAF 2015, Helsinki, Finland*, June 1-5 2015.

[10] Wandong Wang, Calvin Rans, and Rinze Benedictus. Analytical prediction model for fatigue crack growth in fibre metal laminates with msd scenario. *International Journal of Fatigue*, 104:263–272, 2017.

[11] Wandong Wang. *Multiple-site damage crack growth behaviour in Fibre Metal Laminate structures*. PhD thesis, Delft University of Technology, Delft, the Netherlands, 2017.

[12] Zhinan Zhang, Wandong Wang, Calvin Rans, and Rinze Benedictus. An experimental investigation into pin loading effects on fatigue crack growth in fibre metal laminates. *Procedia Structural Integrity*, 2:3361–3368, 2016.

[13] Wandong Wang, Calvin Rans, Zhinan Zhang, and Rinze Benedictus. Prediction methodology for fatigue crack growth behaviour in fibre metal laminates subjected to tension and pin loading. *Composite Structures*, 182:176–182, 2017.

[14] J. J. M. De Rijck. *Stress analysis of fatigue cracks in mechanically fastened joints: an analytical and experimental investigation*. PhD thesis, Delft University of Technology, Delft, the Netherlands, 2005.

[15] J. Schijve. Some elementary calculations on secondary bending in simple lap joints. Nlr-tr-72036, National Aerospace Laboratory, Amsterdam, 1972.

[16] G. Caprino, A. Squillace, G. Giorleo, L. Nele, and L. Rossi. Pin and bolt bearing strength of fibreglass/aluminium laminates. *Composites Part A: Applied Science and Manufacturing*, 36(9):1307–1315, 2005.

[17] Po-Ching Yeh, Po-Yu Chang, Justin Wang, Jenn-Ming Yang, Peter H. Wu, and Ming C. Liu. Bearing strength of commingled boron/glass fiber reinforced aluminum laminates. *Composite Structures*, 94(11):3160 – 3173, 2012.

[18] R.G.J. Van Rooijen, J. Sinke, T.J. De Vries, and S. Van Der Zwaag. The bearing strength of fiber metal laminates. *Journal of Composite Materials*, 40(1):5–19, 2006.

[19] R. M. Frizzell, C. T. McCarthy, and M. A. McCarthy. An experimental investigation into the progression of damage in pin-loaded fibre metal laminates. *Composites Part B: Engineering*, 39(6):907–925, 2008.

[20] R. M. Frizzell, C. T. McCarthy, and M. A. McCarthy. A comparative study of the pin-bearing responses of two glass-based fibre metal laminates. *Composites Science and Technology*, 68(15–16):3314–3321, 2008.

[21] S. Pitt and R. Jones. Multiple-site and widespread fatigue damage in aging aircraft. *Engineering Failure Analysis*, 4(4):237 – 257, 1997.

[22] Jianyu Zhang, Rui Bao, Xiang Zhang, and Binjun Fei. A probabilistic estimation method of multiple site damage occurrence for aircraft structures. *Procedia Engineering*, 2(1):1115 – 1124, 2010. Fatigue 2010.

[23] J.C. Newman and R. Ramakrishnan. Fatigue and crack-growth analyses of riveted lap-joints in a retired aircraft. *International Journal of Fatigue*, 82(Part 2):342 – 349, 2016. 10th Fatigue Damage of Structural Materials Conference.

[24] Yajun Chen, Shengjie Sun, and Chunming Ji. Analysis of aluminum sheets with multiple sites damage based on fatigue tests and {DIC} technique. *International Journal of Fatigue*, 109:37 – 48, 2018.

[25] R. Eastin. 'wfd'-what is it and what's 'lov' got to do with it? *International Journal of Fatigue*, 31:1012–1016, 2009.

[26] Russell J.H. Wanhill. Chapter two - fatigue requirements for aircraft structures. In Rhys Jones, Alan Baker, Neil Matthews, and Victor Champagne, editors, *Aircraft Sustainment and Repair*, pages 17 – 40. Butterworth-Heinemann, Boston, 2018.

[27] C. D. Rans. 2 - bolted joints in glass reinforced aluminium (glare) and other hybrid fibre metal laminates (fml). *in Composite Joints and Connections*, 2011.

[28] J. Schijve. *Fatigue of Structures and Materials*. Kluwer Academic Kluwer Academic Publishers., Dordrecht, 2008.

[29] J. J. M. De Rijck. *Stress analysis of fatigue cracks in mechanically fastened joints: an analytical and experimental investigation*. PhD thesis, Delft University of Technology, Delft, the Netherlands, 2005.

[30] R.P.G. Müller. *An experimental and analytical investigation on the fatigue behaviour of fuselage riveted lap joints : the significance of the rivet squeeze force, and a comparison of 2024-T3 and glare 3*. PhD thesis, Delft University of Technology, Delft, the Netherlands, 1995.

[31] Wandong Wang, Calvin Rans, and Rinze Benedictus. Analytical prediction model for non-symmetric fatigue crack growth in fibre metal laminates. *International Journal of Fatigue*, 103:546–556, 2017.

[32] H. Tada, P. C. Paris, and G. R. Irwin. *The stress analysis of cracks handbook*. ASME, New York, 2000.

[33] Ad Vlot and J. W. Gunnink. *Fibre Metal Laminates-An Introduction*. Kluwer Academic Publisher, Dordrecht, The Netherlands, 2001.

[34] ASTM E647-00. *Standard test method for measurement of fatigue crack growth rates*. ASTM International, 2011.